

See discussions, stats, and author profiles for this publication at: <https://www.researchgate.net/publication/230878129>

Influence of the Length of Imogolite-Like Nanotubes on Their Cytotoxicity and Genotoxicity toward Human Dermal Cells

ARTICLE in CHEMICAL RESEARCH IN TOXICOLOGY · SEPTEMBER 2012

Impact Factor: 3.53 · DOI: 10.1021/tx3003214 · Source: PubMed

CITATIONS

11

READS

75

13 AUTHORS, INCLUDING:



Antoine Thill

Atomic Energy and Alternative Energies Com...

74 PUBLICATIONS 1,308 CITATIONS

[SEE PROFILE](#)



Armand Masion

Centre Européen de Recherche et d'Enseigne...

99 PUBLICATIONS 2,251 CITATIONS

[SEE PROFILE](#)



Alain Botta

Aix-Marseille Université

134 PUBLICATIONS 1,766 CITATIONS

[SEE PROFILE](#)



Jean-Yves Bottero

Centre Européen de Recherche et d'Enseigne...

232 PUBLICATIONS 7,547 CITATIONS

[SEE PROFILE](#)

Influence of the Length of Imogolite-Like Nanotubes on Their Cytotoxicity and Genotoxicity toward Human Dermal Cells

Wei Liu,^{†,‡} Perrine Chaurand,^{†,‡} Carole Di Giorgio,[§] Michel De Méo,[§] Antoine Thill,^{||,‡} Mélanie Auffan,^{†,‡} Armand Masion,^{†,‡} Daniel Borschneck,[†] Florence Chaspoul,[§] Philippe Gallice,[§] Alain Botta,[§] Jean-Yves Bottero,^{†,‡} and Jérôme Rose*,^{†,‡}

[†]CEREGE, UMR 7330, CNRS-Aix Marseille University, BP 80, 13545 Aix en Provence, France

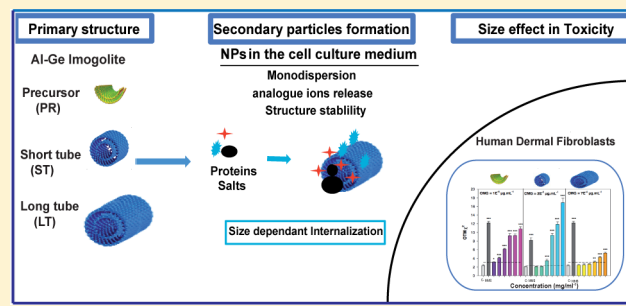
[‡]GDRI iCEINT, International Consortium for the Environmental Implications of NanoTechnology

[§]IMBE, UMR, CNRS, Aix-Marseille University, BP 80 13545, Aix en Provence, France

^{||}CEA, IRAMIS, Laboratoire Interdisciplinaire sur l'Organisation Nanométrique et Supramoléculaire, 911191 Gif-sur Yvette, France

Supporting Information

ABSTRACT: Physical–chemical parameters such as purity, structure, chemistry, length, and aspect ratio of nanoparticles (NPs) are linked to their toxicity. Here, synthetic imogolite-like nanotubes with a set chemical composition but various sizes and shapes were used as models to investigate the influence of these physical parameters on the cyto- and genotoxicity and cellular uptake of NPs. The NPs were characterized using X-ray diffraction (XRD), small angle X-ray scattering (SAXS), and atomic force microscopy (AFM). Imogolite precursors (PR, ca. 5 nm curved platelets), as well as short tubes (ST, ca. 6 nm) and long tubes (LT, ca. 50 nm), remained stable in the cell culture medium. Internalization into human fibroblasts was observed only for the small particles PR and ST. None of the tested particles induced a significant cytotoxicity up to a concentration of 10^{-1} mg·mL⁻¹. However, small sized NPs (PR and ST) were found to be genotoxic at very low concentration 10^{-6} mg·mL⁻¹, while LT particles exhibited a weak genotoxicity. Our results indicate that small size NPs (PR, ST) were able to induce primary lesions of DNA at very low concentrations and that this DNA damage was exclusively induced by oxidative stress. The higher aspect ratio LT particles exhibited a weaker genotoxicity, where oxidative stress is a minor factor, and the likely involvement of other mechanisms. Moreover, a relationship among cell uptake, particle aspect ratio, and DNA damage of NPs was observed.



INTRODUCTION

Nanomaterials are used extensively in a number of fields (health, automotive, personal care, etc.) because of their novel and/or enhanced physical–chemical properties. However, questions have been raised concerning potential toxicological effects of these nanomaterials toward humans and ecosystems. Carbon nanotubes (CNTs) are an emblematic case in this regard. Because of their specific physical–chemical and electrical properties, they are useful for medical, manufacturing, and energy applications.^{1–3} However, *in vivo* and *in vitro* studies revealed the toxicity of these compounds.^{4–7}

Several authors have shown that these materials have a toxicity similar to that of asbestos fibers. They can reach the pleura, where long fibers accumulate, and cause inflammation and fibrosis. Then, there is a risk of developing mesothelioma and genotoxic activity.^{5,8,9} A dose–response relationship has been shown for chromosomal damage induced by multiwall carbon nanotubes.^{4,7} However, it has been reported that high purity single-wall carbon nanotubes did not cause any DNA strand breakages or an increase in mutation frequencies,^{10,11}

whereas less pure single-wall CNTs with similar lengths induced significant DNA damage.^{12,13}

However, clear conclusions on the toxicity mechanisms cannot be drawn because of the variability of the CNTs used, especially in terms of preparation methods, structural integrity, and presence of impurities. To circumvent this difficulty, the question of the toxicity of high aspect ratio nanotubes has been addressed in the present work with a material where only size and shape were allowed to vary, viz., imogolite-like nanotubes. Imogolites are naturally occurring nanotubular aluminosilicates $[(OH)_3Al_2O_3SiOH]$ with a diameter of 2 nm and lengths ranging from a few nm to several hundreds nm.^{14,15} Imogolite is readily obtained by an aqueous phase synthesis (e.g., ref 16) and shows great promise for numerous applications such as optics, catalysis, and gas storage.^{17,18} The Ge analogue of imogolite is obtained with an equally simple aqueous synthesis.^{19,20} Substitution of the silicon atoms by germanium atoms allows one to obtain high yields of nanotubes isostructural to imogolite.

Received: July 16, 2012

Published: September 18, 2012



Depending on the initial concentration of Al and Ge, single- or double-walled Ge imogolites are obtained.²¹ The aspect ratio of these nanotubes can be controlled as a function of the growth stage.²⁰ Additionally, high purity compounds with constant chemical composition are obtained (absence of catalysts during the synthesis), which warrants artifact free toxicity experiments. Three synthetic and fully characterized aluminogermanate nanoparticle types (Al–Ge NPs) were used in the present study to investigate the toxicity of nanotubes: protoimogolite (PR), a roof tile shaped particle, which is the precursor for the subsequent growth of tubular structures,^{20,22} short tubes (ST), and long tubes (LT).

To the best of our knowledge, only one study addresses to date the biological impact of synthetic imogolite nanotubes. It showed good growth and differentiation of osteoblastic cells in the presence of an imogolite scaffolding.²³ In the present work, the goal is to investigate the potential cytotoxicity and genotoxicity of the imogolite-like material (PR, ST, and LT) toward normal human dermal fibroblast. The physical–chemical properties of the NPs were monitored throughout the experiments to better understand the mechanism(s) of toxicity.

MATERIALS AND METHODS

Materials. Ge-imogolite was synthesized according to Levard et al.²⁰ Tetraethoxygermanium is added to an aluminum perchlorate solution (10^{-1} mol/L) with an Al/Ge ratio set to 2. The mixture is slowly hydrolyzed by the addition of a NaOH solution (10^{-1} mol/L) with the rate of flow at $1.5 \text{ mL}\cdot\text{min}^{-1}$ to reach the hydrolysis molar ratio $[\text{OH}]/[\text{Al}]$ of 2. The precursor of imogolite (PR) was formed after the hydrolysis step. Then the mixture was maintained at 95°C for 5 (ST) and 10 days (LT). At the end of the aging step, each sample was dialyzed against ultrapure water for five days by using 1000 Da membranes. The characterization of the structure and the morphology synthesis samples were performed by XRD, SAXS, and AFM (see Supporting Information).

Normal Human Fibroblast Culture. Normal human fibroblasts were isolated by the outgrowth method using infant foreskin obtained after circumcisions.²⁴ The dermis was cut into $0.5\text{--}1 \text{ mm}^3$ pieces under sterile conditions. The small tissue pieces were seeded in culture dishes and incubated in Dulbecco's modified Eagle's medium (DMEM) supplemented with 10% fetal calf serum (FCS), 2 mM L-glutamine, 1 mM sodium pyruvate, 100 U/mL penicillin, and 100 $\mu\text{g}/\text{mL}$ streptomycin. Fibroblasts were then cultured in complete DMEM (cDMEM) without antibiotics at 37°C in a humidified atmosphere containing 5% CO_2 . The culture medium was replaced every two days. Fibroblast cultures were obtained within two weeks.

Size, Zeta Potential, and Dissolution Assessment of NPs in Culture Medium. The hydrodynamic diameter (determined by dynamic light scattering) and the zeta potential of NPs were measured using a Malvern Zetasizer. The samples were diluted in the culture medium and in 10 mM NaCl for a final concentration at $0.1 \text{ mg}\cdot\text{mL}^{-1}$. The measurements were performed after 2 h of incubation under standard cell culture conditions.

Aluminum and germanium release from the particle suspension was measured by ICP-MS (Thermo X series II model equipped with a collision cell). Samples were prepared by diluting the stock particle suspension in complete culture medium at a concentration of $0.1 \text{ mg}\cdot\text{mL}^{-1}$. The incubation was performed for 2 and 24 h under standard cell culture conditions (37°C , 5% CO_2 , 95% humidity). After incubation, aliquots (8 mL) of the particle suspensions were centrifuged at 214,200g for 6 h (Beckman Coulter, optimal L-100 × P ultracentrifuge), and the collected supernatant was diluted 10-fold in ultrapure water ($18 \text{ M}\Omega$) with 1% nitric acid before analysis. Results were expressed as the percentage of the tested suspension.

Structure of NPs in Culture Medium by Using X-ray Absorption Spectroscopy (XAS). Germanium K-edge XAS experiments

were performed at the European Synchrotron Radiation Facility (Grenoble, France) on the FAME beamline (BM30b) with a Si(220) monochromator.^{25,26} After 2 h of incubation, the NP suspension ($0.1 \text{ mg}\cdot\text{mL}^{-1}$) in complete culture medium was freeze-dried. Samples were pressed into thin pellets and cooled to about 10 K during spectra acquisition to decrease thermal motion of atoms. XAS spectra were scanned using a step-by-step mode from 100 to 800 eV above the Ge K-edge. Multiple scans (3–10) were collected for each sample. EXAFS (extended X-ray fine structure) data were obtained after performing standard procedures for pre-edge subtraction, normalization, polynomial removal, and wave vector conversion using the IFEFFIT software package.²⁷ For each atomic shell, the interatomic distance (R), the coordination number (CN), and mean squared displacement (ss^2) were adjusted. The amplitude reduction factor and the threshold position were fit to data from reference compounds (GeO_2) and fixed for all subsequent analyses.

Transmission Electron Microscopy (TEM) Analysis of Cells. Fibroblasts were plated in 6-well plates (5×10^4 cells/well) and incubated at 37°C . After 24 h, the cells were treated with $0.1 \text{ mg}\cdot\text{mL}^{-1}$ of particles. The cells were washed two times in the culture medium to remove all noninternalized particles and then were fixed with 4% of glutaraldehyde in 0.1 M sodium cacodylate buffer for 30 min at 4°C . After postfixation (2% OsO_4 in 0.1 M sodium cacodylate buffer for 1 h at 4°C), the samples were embedded in epoxy resin. Ultrathin sections (60 nm) were obtained with an ultramicrotome. These sections were stained with 8% uranyl acetate solution in 0.5% acetic acid and plumbic citrate, and then placed on 150 mesh copper grids. Morphologic characteristics of the cells and the distribution of particles within the cells were analyzed with a JEOL/JEM-1220 electron microscope operated at 80 kV. Energy dispersive X-ray detector (EDAX Genesis) was used to carry out the chemical analysis.

Cell Uptake of NPs. To quantify the NPs associated with/taken up by cells, the fibroblasts were seeded in a six-well culture plate (Falcon, Milan, Italy) with a density of 1×10^6 cells per well. Twenty-four hours after seeding, the cells were treated with PR, ST, and LT at concentrations of 1×10^{-1} , 1×10^{-2} , and $1 \times 10^{-3} \text{ mg}\cdot\text{mL}^{-1}$ for 2 and 24 h. At the end of incubation, the samples were centrifuged at 214,200g for 6 h. The supernatant was collected for the comet assay (see below). The cells were rinsed twice with PBS and then trypsinized. The solution containing the cells was centrifuged and the cells resuspended in Milli-Q water containing 0.1% Triton X100 for ICP-MS analysis.

Toxicity Assessment. Cytotoxicity Assay. The WST-1 assay was used to characterize mitochondrial activity in response to the NP samples. Cells (20,000 cells/well) were seeded in 96-well plates and incubated overnight at 37°C in a humidified atmosphere containing 5% CO_2 . After 2 and 24 h, the medium was changed, and 200 μL of fresh medium containing the compound to be tested was added to obtain final NP concentrations between 1×10^{-1} to $1 \times 10^{-6} \text{ mg}\cdot\text{mL}^{-1}$. At the end of the incubation period, the cultures were washed 3 times in phosphate buffered saline (PBS) and incubated for an additional 30 min in fresh culture medium containing 10% WST-1. Cell viability was evaluated by the assessment of WST-1 absorbance at 450 nm in a microplate spectrophotometer MRX II (Dynex Technologies, Chantilly, VA, USA).

The NRU dye assay measures the accumulation of the neutral red dye in the lysosomes of viable cells. At the end of two incubation periods (2 and 24 h), the medium was removed, and 200 μL of neutral red dye ($50 \mu\text{g}\cdot\text{mL}^{-1}$) dissolved in serum free medium was added to each well. After incubation at 37°C for 3 h, the cells were washed with PBS, and the internalized dye by cells was then dissolved in 200 μL of fixation solution (1% acetic acid, 50% ethanol, and 49% ultrapure water) and added to each well. Absorbance was monitored at 540 nm.

Alkaline Comet Assay. A modified version of the standard alkaline comet assay has been used in the present study.²⁸ Fibroblasts (1×10^5 cells/well in a six-well plate) were incubated in duplicate for 2 h with each subset of nanoparticles at concentrations from 1×10^{-1} to $1 \times 10^{-6} \text{ mg}\cdot\text{mL}^{-1}$. Untreated cells were used as negative control to determine background DNA-damage levels. The positive control was methylmethanesulfonate (MMS, 60 μM), which is a well-known

genotoxic compound. At the end of the incubation period, the cells were transferred to microscope slides coated with two agarose layers and lysed in a detergent solution for 90 min at 8 °C. DNA unwinding was carried out with an alkaline solution for 20 min at room temperature. Then, electrophoresis was conducted for 20 min (25 V, 300 mA) in the same buffer solution. After electrophoresis, the slides were neutralized, dried at room temperature, and stained with 50 µL of ethidium bromide solution (2 µg·mL⁻¹). The slides were examined under a fluorescence microscope (250×). Image analysis was performed using the Komet software (version 5.5; Kinetics Imaging, Nottingham, UK) on 100 randomly selected cells from duplicate slides. DNA damage was expressed as olive tail moment (OTM, arbitrary units).²⁸ The calculated OTM values were distributed into 40 classes between the minimal and the maximal OTM values. A nonlinear regression analysis was performed on the normalized distribution frequencies using a χ^2 function with TableCurve 2D (version 5.0; Jandel Scientific Software, San Rafael, CA). The calculated level of freedom (n) for the function, named OTM χ^2 , was assumed to be a quantitative measure of the level of DNA damage in the sample.²⁹

ERT Treatment. The genotoxic effects of reactive oxygen species (ROS) were evaluated on cells pretreated with 4 mM ERT for 1 h at 37 °C. After incubation, the cells were washed with PBS buffer. The samples at various concentrations were added, and the comet assay was performed. Cells exposed to 120 kJ/cm² UVA irradiation for 3 min with and without ERT were used as controls.

Micronucleus Assay. The ability of nanoparticles to induce micronuclei was assessed following the protocol described by Kirsch-Volders et al.³⁰ A total of 100,000 cells were plated in chamber slides and incubated for 24 h at 37 °C in a humidified atmosphere containing 5% CO₂. The concentrations of nanoparticles in duplicate cell cultures ranged from 1×10^{-1} to 1×10^{-6} mg·mL⁻¹. A culture medium control was used to determine the background DNA-damage levels in cells. Positive controls with a well-known genotoxic compound, i.e., 0.06 µg·mL⁻¹ mitomycin C (MMC, Sigma, St Quentin-Fallavier, France), were included to ensure the sensitivity of the assay. After 24 h of exposure, cells were rinsed with PBS and incubated for an additional 24 h in a fresh medium containing cytochalasin B (3 µg·mL⁻¹) to stop cytokinesis. At the end of the incubation period, the cells were washed twice with PBS and fixed with methanol (HPLC grade solvent). The slides were air-dried and stained with 5% Giemsa stain in Milli-Q water for 15 min.

The micronucleated cell rates were determined for concentrations inducing less than a 50% decrease in the proliferative index: 2000 binucleated cells were examined, and micronuclei were identified according to the morphological criteria.³¹ Statistical differences between negative controls and treated samples were determined using the χ^2 test. The assay was considered positive when a dose-response relationship could be established between the numbers of micronucleated cells and the concentrations of nanoparticles and when at least one concentration induced a significant increase of micronucleated cells as compared to the control culture.

RESULTS AND DISCUSSION

Structural Characterization of NPs. The three Al–Ge NP types were characterized by combining three techniques XDR, SAXS, and AFM (see Supporting Information). The XRD patterns (Figure S1A, Supporting Information), whose bands have been described earlier,^{19,32} show a quasi identical local structure among the NP samples. In particular, the 8.5 Å repeat distance along the *c*-axis of the nanotube is clearly visible for the tubular structures ST and LT. At the larger scale, SAXS data (Figure S1B, Supporting Information) show oscillations at high *Q* that are characteristic for a ring/tube structure in the case of ST and LT. The SAXS curve of the PR sample, which does not display this feature, is easily fitted by roof tile shaped fragments²⁰ which assemble into a doughnut type structure upon further aging. The ST and LT samples show the characteristic oscillations of double wall nanotubes.²¹ In these

cases, the best fits were obtained with models of nanotubes with 4.3 and 1.4 nm outer- and inner wall diameter, respectively, and a wall thickness of 6 Å. Tube lengths are ca. 6 nm for ST and ≥35 nm (i.e., the low *q* limit of our experimental set up) for LT. The scattering is also proportional to the nanotube concentration. The number concentrations estimated from the SAXS data are 3.05×10^{16} nanotubes/cm³ for ST and 5.4×10^{15} nanotubes/cm³ for LT.

AFM images (Figure S2, Supporting Information) provided the length distribution of the nanotubes. Because of the convolution with the tip shape, a minimum tube length of 10 nm is necessary to differentiate two tubes. For this reason, the size distribution was determined only for the LT sample. The LT sample displayed an average length at 51 nm and a broader distribution (40 nm). ST length was 10 nm or below, with an estimated average length around 6 nm (Table 1).

Table 1. Calculated Parameters of the NPs Used

	<i>L</i> (nm)	<i>D</i> outer wall (nm)	wall thickness (Å)	calculated no. of particle in 1 g L ⁻¹	calculated surface specific area (m ² g ⁻¹)
PR	5		5		1749
ST	6 ± 4	4.3	6	3.5×10^{18}	960
LT	51 ± 40	4.3	6	9.8×10^{17}	648

Behavior of NPs in the Cell Culture Medium and in Contact with Cells. Dynamic light scattering indicated that the three suspensions were quasi monodisperse and remained stable up to 2 h of incubation in the cell culture media (cDMEM, pH 7.8) (Figure 1A). Indeed, when the particles (1×10^{-1} mg·mL⁻¹) were added to the cDMEM medium, distributions of hydrodynamic diameter observed for PR and ST were centered at 8 nm. The distribution of the hydrodynamic diameter for LT was centered at larger value, i.e., 30 nm. This agrees with previous reports showing that the presence of a complex mixture of proteins in the cell medium is an effective dispersing agent through the adsorption of proteins at the surface of NPs.^{33,34} Moreover, under physiological conditions, most proteins showed anionic properties.³⁵ Protein sorption is most likely the reason why the initially positive zeta potential of all our NPs decreased to -10 mV within 1 min and remained unchanged for up to 2 h (Figure 1B).

Partial dissolution of NPs can release toxic metal ions. In our case, the release of Al and Ge ions after 2 h of incubation was low, viz., typically <2% of the initial concentrations for all NP types (Figure 2). After a 24 h incubation period, the released Al and Ge quantities were higher: PR exhibited the highest dissolution rate (Al, 9.7%; Ge, 8.8%), ST (Al, 4.1%; Ge, 2.0%) and LT (Al, 2.3%; Ge, 1.5%) being less affected by the prolonged incubation. Moreover, the molar ratio of free Al and Ge atoms from tubular samples was about 2, which was close to the ratio of the synthetic product and reflected the congruent dissolution.

Structural defects in multiwalled carbon nanotubes can play a major role in the genotoxicity of epithelial cells.⁵ To take into account this hypothesis, the structural integrity of our NP samples in cDMEM was determined by examining the coordination environment around Ge. The $k^3\text{-chi}(k)$ Ge K-edge EXAFS spectra of all the samples are similar (Figure 3). In all cases, the first atomic sphere corresponded to the oxygen of the 4-fold coordinated Ge (Table 2).¹⁹ For ST and LT, the presence of ca. 6 of Al atoms in the next nearest shell is consistent with the

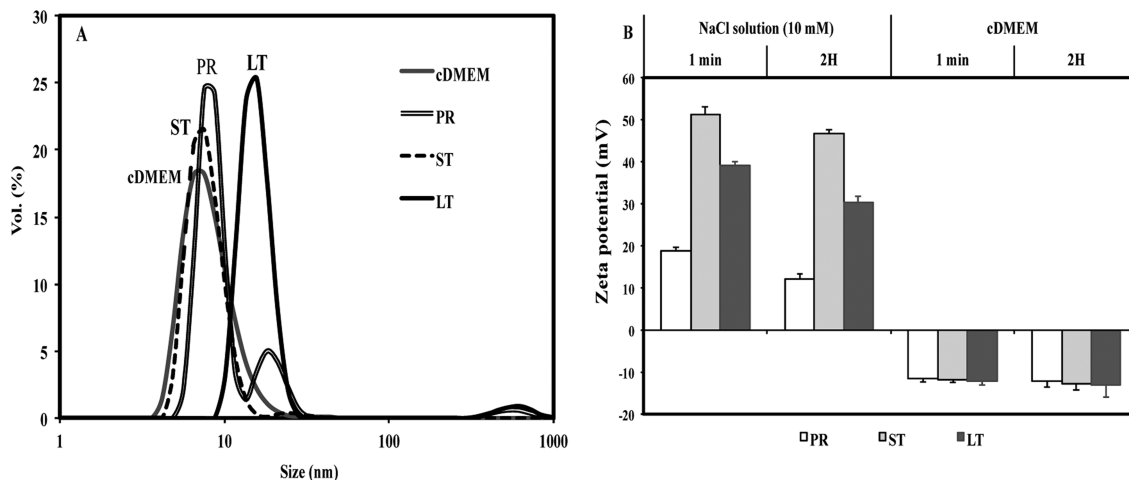


Figure 1. Size distribution and zeta potential measurement of NPs in cDMEM. (A) DLS analysis of NPs (10^{-1} mg/mL $^{-1}$). (B) Zeta potential measurement of NPs (10^{-1} mg/mL $^{-1}$) in 10 mM NaCl solution (pH \approx 7.8) and cDMEM.

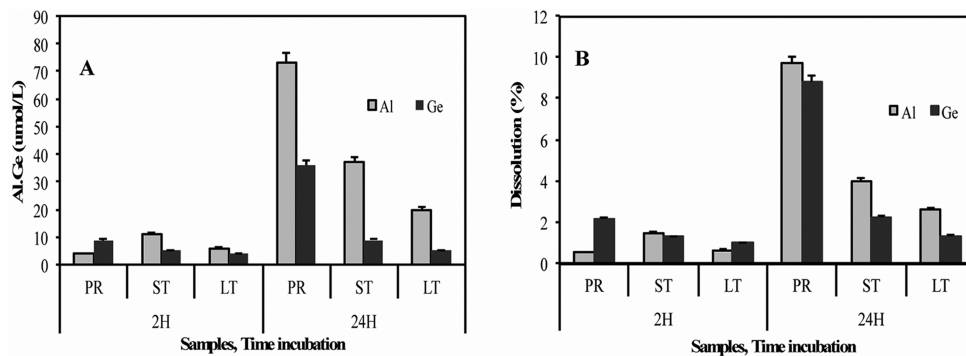


Figure 2. NP dissolution in cDMEM. Concentration (A) and percentage (B) of Al ions and Ge ions released from 10^{-1} mg·mL $^{-1}$ of NP suspension after 2 and 24 h of incubation in cell culture medium measured by ICP-MS.

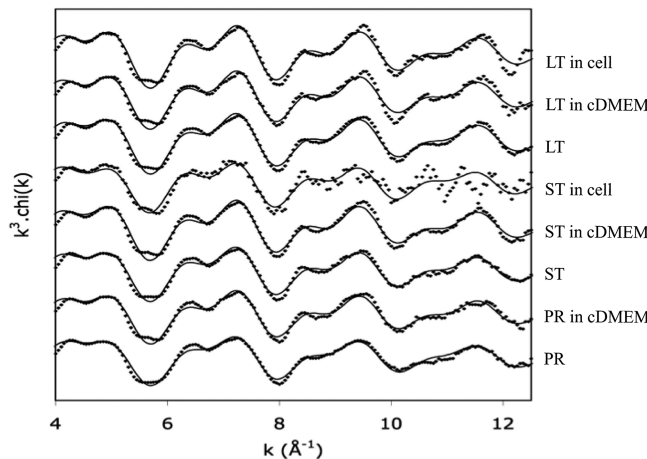


Figure 3. Ge K-edge EXAFS spectra of PR, ST, and LT incubated for 2 h in cDMEM. PR, ST, and LT refer to the reference particles. Dotted line: experimental data. Solid line: calculated.

theoretical structure of fully formed Ge-imogolite. For PR, however, the number of Al neighbors is significantly lower and indicates defects in the Gibbsite layer, as described previously.²⁰ The most important finding, however, is that the initial local scale structure of the NPs is not modified in the cDMEM culture medium and by cell contact (Table 2) and, as a consequence, that, in our case, differences in biological effects can

Table 2. Model Fitting Parameters: Coordination Number (CN), Interatomic Distance (R), and Mean Squared Displacement (ss^2) for Ge K-edge EXAFS Data Shown in Figure 3^a

samples	Ge–O shell			Ge–Al shell		
	CN	R	ss^2	CN	R	ss^2
PR	4.1	1.77	0.004	4.0	3.26	0.006
PR DMEM	4.1	1.76	0.003	5.2	3.26	0.003
ST	4.2	1.77	0.004	5.4	3.26	0.006
ST DMEM	4.4	1.76	0.004	6.2	3.27	0.006
ST cell	3.9	1.78	0.004	5.3	3.26	0.006
LT	4.7	1.76	0.004	5.9	3.26	0.006
LT DMEM	4.3	1.76	0.004	6.2	3.26	0.006
LT cell	4.5	1.76	0.004	6.7	3.26	0.006

^aFit range: $k = 3.8$ – 12.6 Å $^{-1}$. Errors: (CN) \sim 20% – (R) \sim 0.02 Å; (ss^2) \sim 0.001 Å 2 . The Ge–O and Ge–Al shells correspond to oxygen atoms present in the first coordination sphere and aluminum atoms in the second coordination sphere, respectively.

be linked directly to differences in the aspect ratio of the starting material.

Cell Uptake of NPs. Size and shape of a material have a strong influence on the cellular uptake: high-aspect ratio particles were internalized faster than their low-aspect ratio counterparts.³⁶ Similarly, the mechanism of cellular uptake and removal of protein-coated gold NPs was found to depend on their size and shape.³⁷

In this work, internalization of NPs was investigated by TEM of the fibroblasts (Figure 4). All 3 types of NPs sorbed onto the

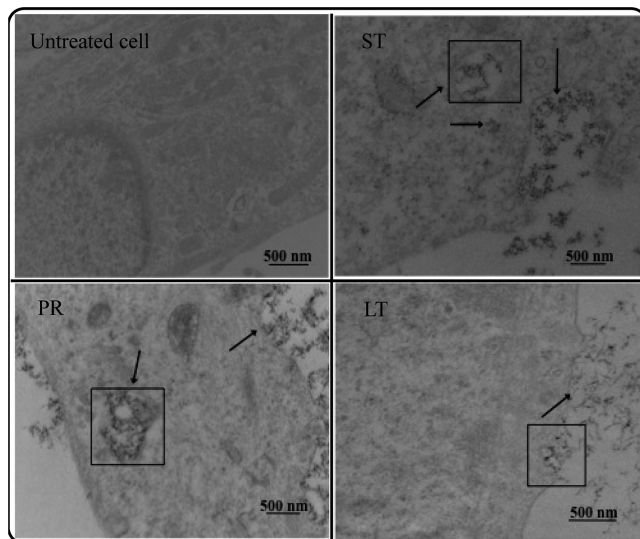


Figure 4. TEM pictures and EDX patterns. Untreated cell and human fibroblasts incubated for 2 h with $100 \mu\text{g}\cdot\text{mL}^{-1}$ of precursor (PR): the limits of the vesicle are not well-defined and seem to be disrupted. Short tube (ST), the beginning of an endocytosis process seems to take place (see arrow); long tube (LT), adsorption of nanofibers onto the external cell membrane. EDX spectra confirmation of the presence of NPs in the vesicle area. The characteristic peaks of Ge and Al were observed. Other elements observed in the spectra correspond to fixation and staining materials.

external cell membrane in the form of aggregates during the incubation with fibroblasts. PR altered the cell morphology with the disruption of the cell membrane. In the case of ST and LT, the cells remained intact (Figure 4). Interestingly, cells treated with PR and ST samples showed the presence of vesicles in the cytoplasm, which contained individual and/or aggregated particles. In these vesicles, NP clusters were 100–300 nm in diameter. The presence of NPs was also confirmed by EDX analysis (Figure S3, Supporting Information). No NPs were detected inside mitochondria, the endoplasmic reticulum, or the Golgi apparatus. The cells exposed to LT did not display vesicles. ICP-MS determinations of Al and Ge showed that, in all cases, increasing the incubation time and/or the initial NPs concentration resulted in higher NP uptake (Figure 5). These data also revealed a clear trend: ST has a higher affinity toward fibroblasts than PR and LT, even though the differences between the types of NP vanished at the highest exposure concentration and longest incubation times. Thus, the length played a critical role in the cell internalization of NPs under our experimental conditions. Since ST and LT are isostructural, differences in uptake rates can be related to their aspect ratio. Previous findings describe higher internalization rates³⁶ and greater impact on cell functions in the case of high aspect ratio material.^{38–40} With the Ge-imogolite NP in the present work, the opposite trend was observed. To the best of our knowledge, this is the first report indicating a preferential uptake of a low aspect ratio fiber.

A possible explanation for this different cell uptake could be attributed to the NP–protein interaction. PR and ST could adsorb more proteins than LT due to their reactive surface properties. NPs with more surface proteins might have a higher

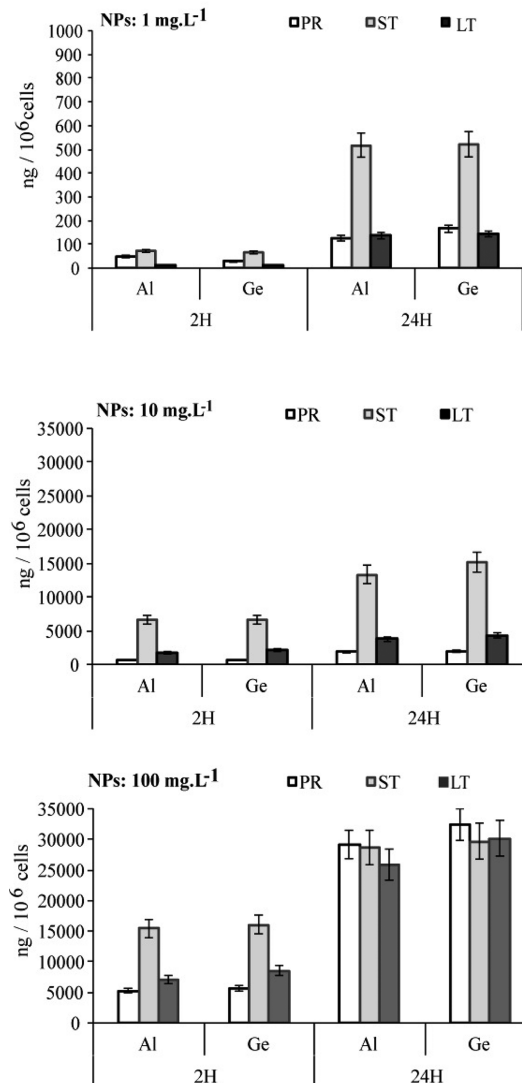


Figure 5. Uptake/associated Al and Ge analysis of fibroblasts via ICP-MS. Cells treated with NPs at the 2 h and 24 h incubation time period. The results are presented as ng of Al or Ge per 1×10^6 cells.

capacity to expose ligands to the membrane receptors and thus might facilitate their internalization.^{41,42}

Cytotoxicity and Genotoxicity of NPs. To determine whether the observed differences in particle size and shape of samples result in a differential cytotoxic potential to fibroblasts, the WST-1 (mitochondrial activity) and NRU (lysosomal capacity) assays were performed with all three NP types. With one exception (WST-1 with ST at $0.1 \text{ mg}\cdot\text{mL}^{-1}$, i.e., the highest tested concentration, 24 h incubation), none of the tests showed significant diminution of cell viability (Figure 6). Furthermore, no differences between the NP types were observed in the cell responses. Two independent assays demonstrated the absence of an acute cytotoxicity induced by Ge-imogolite NPs, even at the highest concentration. The observed differences in cell uptake do not lead to differences in cell viability (Figure 6).

Since none of the Ge-imogolite NPs caused significant cytotoxicity, our focus went to examining possible differences in the genotoxic potentials of the three particle types PR, ST, and LT. In the alkaline comet assay, DNA strand-break analyses were compared to a negative control (untreated fibroblasts) and a well-known genotoxic agent (MMS, $60 \mu\text{g}\cdot\text{mL}^{-1}$). The three

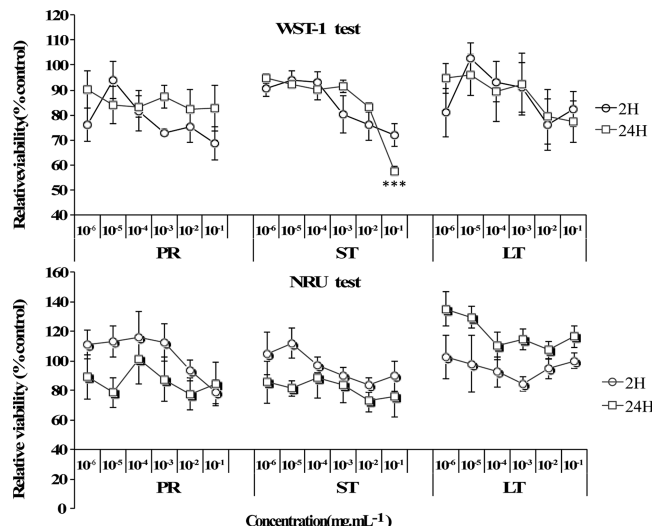


Figure 6. Cytotoxicity assessment. Effect of NPs on fibroblast cells for the 2 h and 24 h period evaluated by the WST-1 test and NRU test. Error bars represent one standard deviation based on triplicate measurements. The statistical significance is determined by Student's *t*-test (***(*p* < 0.001).

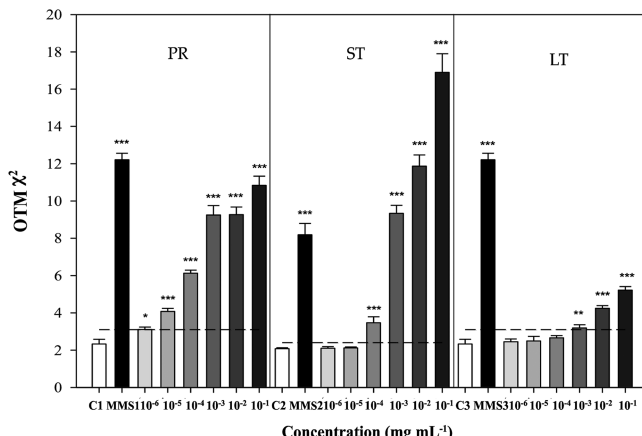


Figure 7. DNA damage evaluated by the comet assay. DNA damage expressed as the OTM χ^2 values, in fibroblasts exposed to different concentrations of PR, ST, and LT (10^{-1} to 10^{-6} mg·mL⁻¹) for 2 h. **P* < 0.05, ** *P* < 0.01, ****P* < 0.001. -----: limit of significance, *P* = 0.05. Statistical differences between negative controls and treated samples were determined using the χ^2 test.

particle types induced statistically significant DNA damage with a dose-response relationship (Figure 7). PR induced a significant DNA damage from the lowest concentration (1×10^{-6} mg·mL⁻¹). The highest concentration tested caused a 4.6-fold increase of OTM χ^2 value compared to the negative control. The short tubes caused even more drastic effects: significant DNA damage was detected from 1×10^{-4} mg·mL⁻¹ and increased with the ST concentration to reach an OTM χ^2 value nearly 10 times higher than that of the negative control. On the contrary, the LT samples, i.e., the particles with the highest aspect ratio, induced only a moderate elevation of the OTM χ^2 value at high concentrations. The minimal genotoxic concentrations (MGC) of PR, ST, and LT were 1×10^{-6} , 2×10^{-5} , and 7×10^{-4} mg·mL⁻¹, respectively. This observation indicated that PR and ST samples induced dose-dependent DNA lesions in fibroblasts from the first tested dose (10^{-6} mg·mL⁻¹) and that LT NPs were less genotoxic. The absence of DNA damage induced supernatants of the NP suspensions (Table 3) clearly demonstrates that the effects observed above are due to the NPs themselves and not released ions.

In general, NPs have been shown to promote DNA damage through a number of direct and indirect mechanisms. After penetrating into the cells, NPs may directly gain access to the nucleus either via diffusion across the nuclear membrane, transport through the nuclear pore complexes, or during mitosis. Alternatively, they may generate oxidative stress, inflammation, and aberrant signaling processes that could lead to DNA damage.⁴³ These lesions can trigger various cellular responses such as cell cycle arrest, apoptosis, and DNA repair. Since unrepaired DNA lesions have been implicated in carcinogenesis, DNA repair is therefore essential to maintain genetic integrity and cell survival, but if repair fails to occur during or before replication of the damaged DNA, this could potentially lead to mutations and therefore cancer.⁴⁴ In this work, the mutagenic potential of Al-Ge NPs was evaluated by using the micronucleus assay to complement the detection of the primary DNA lesions as assessed by the alkaline comet assay. As indicated in Figure 8, PR, ST, and LT induced a dose-dependent and statistically significant increase of micronucleated cell rates. PR and ST displayed the highest clastogenic/aneugenic activities, with a minimal active concentration (MAC) reaching 6.8×10^{-5} and 5.7×10^{-5} mg·mL⁻¹, respectively, whereas LT were far less active (MAC = 7×10^{-3} mg·mL⁻¹).

Table 3. Evaluation of the Dissolution Effect on the Genotoxicity of NPs

sample (conc.)	OTM ^a		% tail DNA ^a		OTM $\chi^2 \pm$ SE ^b
	mean \pm SE	median	mean \pm SE	median	
control	3.81 \pm 0.47	2.56	11.06 \pm 1.13	8.35	2.10 \pm 0.04
MMS (60 μ M)	22.54 \pm 2.04	17.72	29.97 \pm 1.85	28.68	6.16 \pm 0.38***
PR 10^{-3} mg·mL⁻¹	1.80 \pm 0.21	1.03	9.22 \pm 1.16	4.50	2.08 \pm 0.04
PR 10^{-2} mg·mL⁻¹	2.38 \pm 0.26	1.65	9.83 \pm 0.98	6.63	2.10 \pm 0.05
PR 10^{-1} mg·mL⁻¹	2.34 \pm 0.31	1.37	9.64 \pm 1.04	5.79	2.08 \pm 0.03
ST 10^{-3} mg·mL⁻¹	2.16 \pm 0.20	1.81	9.94 \pm 0.89	8.41	2.09 \pm 0.05
ST 10^{-2} mg·mL⁻¹	1.82 \pm 0.20	1.13	9.20 \pm 1.21	5.21	2.07 \pm 0.02
ST 10^{-1} mg·mL⁻¹	2.51 \pm 0.31	1.73	10.55 \pm 1.02	8.93	2.08 \pm 0.03
LT 10^{-3} mg·mL⁻¹	2.15 \pm 0.28	1.49	8.90 \pm 0.87	6.30	2.10 \pm 0.07
LT 10^{-2} mg·mL⁻¹	2.10 \pm 0.21	1.62	9.45 \pm 1.01	6.06	2.08 \pm 0.03
LT 10^{-1} mg·mL⁻¹	2.19 \pm 0.25	1.50	10.75 \pm 1.43	4.46	2.09 \pm 0.06

^aOTM and tail DNA (%) values were determined with the Fenestra Komet software (Kinetics Imaging, Nottingham, UK). Means \pm SD and medians were calculated on 100 cells. ^bOTM χ^2 values were calculated by nonlinear regression analysis using a χ^2 function on the distribution frequencies of OTM as described in Materials and Methods. ***: statistical difference with the control at *P* < 0.001.

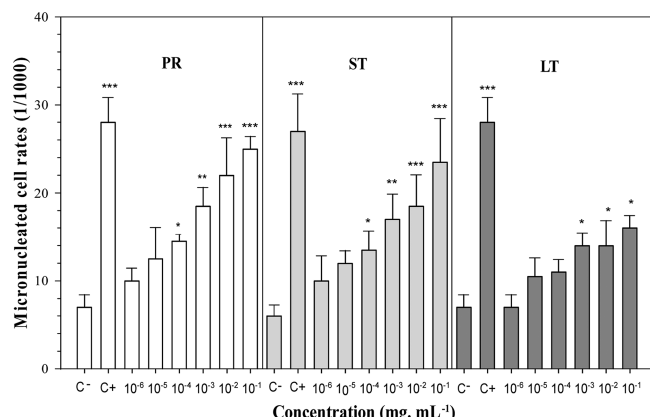


Figure 8. Clastogenic/aneugenetic activities have been observed in NPs by the micronucleus assay. C, control culture; C+, positive control ($0.06 \mu\text{g}\cdot\text{mL}^{-1}$ mitomycin C); ----, significance limit, $P = 0.05$. Statistical differences between negative controls and treated samples were determined using the χ^2 test.

These data indicate that, under our experimental conditions, the two short NPs (PR and ST) induced more DNA damage and clastogenic/aneugenetic activities than the LT samples. Thus, there is a size effect when results are compared in terms of the initial concentration of NPs. However, due to large differences in size, the number of PR, ST, and LT particles for a given concentration is very different. After extrapolation of the genotoxicity values (OTM χ^2) as a function of the mass- and

number concentrations (mg/L and particles/L), we observed that the induction of a significant OTM χ^2 value of 3 corresponded to 2.5×10^{14} particles/L for ST and 4.5×10^{14} particles/L for LT. The ratio of LT/ST is 1.8. However, when expressed in mass concentration, this ratio is 7, i.e., more than 3 times higher (ST, $7 \times 10^{-2} \text{ mg}\cdot\text{mL}^{-1}$; LT, $5 \times 10^{-1} \text{ mg}\cdot\text{mL}^{-1}$) (Figure S4, Supporting Information). This correlation shows that the number of NPs is a useful parameter to understand the observed toxicity and that the differences observed as function of mass concentrations become less marked when the number concentrations are considered.

Size and Surface Properties of NPs Related to the Oxidative Stress.

As reported in the literature, size and surface reactivity of NPs play a key role in the biological response involving various physical and chemical mechanisms. This includes the disruption of membrane activity,^{45,46} changed protein conformation,⁴⁷ and protein aggregation/fibrillation.⁴⁸ In addition, ROS production has been considered as the main chemical mechanism of NP-induced toxicity.^{49–51} Interactions between NPs and cellular membranes or biological macromolecules can induce oxidative stress and then cause cell damage.^{8,52,53}

To address the likelihood of this mechanism here, the oxidative stress induced by our NPs was investigated by using the modified alkaline comet assay with and without pretreatment with ERT. ERT acts as an efficient ROS scavenger to reinforce the cell antioxidant potential.^{54,55} The activity of the ERT was verified by the reduction of 100% of the genotoxicity caused by UV/vis irradiation, known to produce oxidative DNA damage (Table 4).⁵⁶

Table 4. Evaluation of the L-Ergothioneine (ERT) Effect on the Genotoxicity of Nanoparticles^a

sample ^b (concn)	OTM		% tail DNA		OTM $\chi^2 \pm \text{SE}$	% protection
	mean \pm SE	median	mean \pm SE	median		
control	3.78 \pm 0.52	2.30	10.83 \pm 1.16	7.73	2.08 \pm 0.04	
UVA	34.86 \pm 2.94	30.94	32.42 \pm 2.05	32.49	4.23 \pm 0.31***	
control + ERT	5.07 \pm 0.58	3.34	14.57 \pm 1.39	11.18	2.07 \pm 0.02	
UVA + ERT	4.85 \pm 0.62	2.73	12.24 \pm 1.19	9.11	2.07 \pm 0.03	100
PR 10 ⁻⁶	14.66 \pm 1.4	8.55	22.06 \pm 1.87	17.91	2.10 \pm 0.03	
PR 10 ⁻⁵	23.24 \pm 2.0	14.08	27.82 \pm 2.18	22.85	2.12 \pm 0.04	
PR 10 ⁻⁴	24.26 \pm 2.5	17.44	30.85 \pm 1.91	23.46	4.10 \pm 0.19***	
PR 10 ⁻³	34.52 \pm 3.7	19.61	32.78 \pm 2.28	26.47	4.30 \pm 0.20***	
PR 10 ⁻⁶ + ERT	2.92 \pm 0.40	1.38	8.88 \pm 1.03	4.65	2.08 \pm 0.05	NA
PR 10 ⁻⁵ + ERT	2.91 \pm 0.33	1.77	11.06 \pm 1.17	6.84	2.09 \pm 0.07	NA
PR 10 ⁻⁴ + ERT	3.34 \pm 0.65	0.78	8.29 \pm 1.30	2.28	2.05 \pm 0.02	100
PR 10 ⁻³ + ERT	3.09 \pm 0.30	2.56	10.83 \pm 1.09	7.32	2.08 \pm 0.05	99.5
ST 10 ⁻⁴	18.92 \pm 1.3	14.79	29.26 \pm 1.98	27.59	4.15 \pm 0.15***	
ST 10 ⁻³	32.62 \pm 2.5	25.86	31.96 \pm 2.14	30.56	5.99 \pm 0.30***	
ST 10 ⁻²	38.23 \pm 3.9	27.32	33.37 \pm 2.07	31.04	6.26 \pm 0.22***	
ST 10 ⁻⁴ + ERT	4.08 \pm 0.61	2.17	9.71 \pm 1.12	5.84	2.07 \pm 0.04	100
ST 10 ⁻³ + ERT	1.96 \pm 0.39	0.60	6.21 \pm 1.01	1.81	2.07 \pm 0.04	100
ST 10 ⁻² + ERT	3.65 \pm 0.57	2.00	8.95 \pm 0.91	6.04	2.09 \pm 0.07	99.5
LT 10 ⁻³	12.04 \pm 0.8	10.44	24.70 \pm 1.73	23.00	3.11 \pm 0.10***	
LT 10 ⁻²	24.77 \pm 2.9	16.74	27.44 \pm 2.34	25.38	4.13 \pm 0.18***	
LT 10 ⁻¹	29.60 \pm 2.8	22.74	29.76 \pm 1.96	26.74	5.35 \pm 0.24***	
LT 10 ⁻³ + ERT	14.99 \pm 1.7	7.53	20.92 \pm 1.56	18.89	3.47 \pm 0.08***	95.1
LT 10 ⁻² + ERT	15.34 \pm 1.0	11.42	22.15 \pm 1.56	18.89	3.47 \pm 0.08***	31.7
LT 10 ⁻¹ + ERT	32.67 \pm 2.6	23.69	32.65 \pm 2.02	31.14	4.72 \pm 0.30***	19.0

^a% Protection was defined as % protection = $(1 - ((DL - CL)/(D - C))) \cdot 100$ where DL is OTM χ^2 calculated at dilution D in the presence of ERT; CL is OTM χ^2 calculated for the control in the presence of ERT; D is OTM χ^2 calculated at the dilution D; and C is OTM χ^2 calculated for the control. NA: not applicable as no genotoxicity could be detected at the tested dilution. ***: statistical difference with the control at $P < 0.001$. ^bPR (10^{-6} to 10^{-3} $\text{mg}\cdot\text{mL}^{-1}$), ST (10^{-4} to 10^{-2} $\text{mg}\cdot\text{mL}^{-1}$), and LT (10^{-3} to 10^{-1} $\text{mg}\cdot\text{mL}^{-1}$) were tested on fibroblasts with and without the ERT pretreatment (4 mM).

The presence of 4 mM ERT completely inhibited the genotoxic effects of PR and ST samples at 10^{-4} and 10^{-3} mg·mL $^{-1}$. This suggests that oxidative stress is the primary mechanism leading to DNA damages in the case of the two shorter NP types (PR and ST). For the high aspect ratio LT particles, ERT protection was only partial and decreased with increasing LT concentration (Table 4). This shows that for the longer Ge-imogolite tubes, oxidative stress becomes a minor factor in the genotoxic response and that other genotoxic mechanisms are involved.

CONCLUSIONS

Three types of Al–Ge NPs with the same chemical composition but various sizes and shapes were used as models to investigate the influence of these physical parameters on cell uptake as well as the cyto- and genotoxicity of these NPs. NP uptake is higher with the shorter particles (PR and ST), which caused significant lesions of DNA, mainly through oxidative stress. The higher aspect ratio LT particles induced a weaker genotoxicity in which oxidative stress is a minor factor. Finally, whereas the size effect on the amplitude of the genotoxic effects is less apparent when number- instead of mass concentrations are considered, the influence of the aspect ratio on the toxicity mechanism remains clearly marked.

ASSOCIATED CONTENT

Supporting Information

Characterization of the structure and morphology of synthesis of samples: XRD and SAXS patterns, and AFM pictures; EDX pattern confirmation of NPs analysis in selected sample areas; and correlation between NP initial concentration and the tube number/OTM χ^2 ratio. This material is available free of charge via the Internet at <http://pubs.acs.org>.

AUTHOR INFORMATION

Corresponding Author

*Tel: +33 442971529. Fax: +33 442971559. E-mail: rose@cerege.fr.

Funding

Support for this work was provided by ANSES within the French National Program “Environmental and Occupational Health” (Programme national de recherche Environnement-Santé Travail) for the project EST-2010/2/016 “NanotoxIMO” with funds allocated by the French Ministries for the Environment and Labor and by several cofinancers: French Agency for Environment and Energy Management (ADEME), Multi-Organization Thematic Institute for Cancer (ITMO Cancer) as part of the 2009–2013 Cancer Plan, and French National Agency for Water and Aquatic Environments (ONEMA) under the 2018 Ecophyto Plan.

Notes

The authors declare no competing financial interest.

ABBREVIATIONS

NP(s), nanoparticle(s); XRD, X-ray diffraction; SAXS, small angle X-ray scattering; AFM, atomic force microscopy; PR, imogolite precursors; ST, short tubes; LT, long tubes; CNTs, carbon nanotubes; Al–Ge NPs, aluminogermanate nanoparticles; NRU, neutral red uptake; ERT, L-ergothioneine; DMEM, Dulbecco’s modified Eagle’s medium; cDMEM, complete DMEM; XAS, X-ray absorption spectroscopy; EXAFS, extended X-ray fine structure; TEM, transmission

electron microscopy; MMS, methylmethanesulfonate; OTM, olive tail moment; MMC, mitomycin C; ROS, radical oxygen species; DLS, dynamic light scattering; MGC, minimal genotoxic concentrations; MAC, minimal active concentration

REFERENCES

- (1) Bianco, A., Kostarelos, K., Partidos, C. D., and Prato, M. (2005) Biomedical applications of functionalised carbon nanotubes. *Chem. Commun.*, 571–577.
- (2) Gooding, J., Wibowo, R., Liu, J., Yang, W., Losic, D., Orbons, S., Mearns, F., Shapter, J., and Hibbert, D. (2003) Protein electrochemistry using aligned carbon nanotube arrays. *J. Am. Chem. Soc.* 125, 9006–9007.
- (3) Peer, D., Karp, J. M., Hong, S., FaroKhzad, O. C., Margalit, R., and Langer, R. (2007) Nanocarriers as an emerging platform for cancer therapy. *Nat. Nanotechnol.* 2, 751–760.
- (4) Muller, J., Decordier, I., Hoet, P. H., Lombaert, N., Thomassen, L., Huaux, F., Lison, D., and Kirsch-Volders, M. (2008) Clastogenic and aneuploidogenic effects of multi-wall carbon nanotubes in epithelial cells. *Carcinogenesis* 29, 427–433.
- (5) Muller, J., Huaux, F., Fonseca, A., Nagy, J. B., Moreau, N., Delos, M., Raymundo-Pinero, E., Beguin, F., Kirsch-Volders, M., Fenoglio, I., Fubini, B., and Lison, D. (2008) Structural defects play a major role in the acute lung toxicity of multiwall carbon nanotubes: toxicological aspects. *Chem. Res. Toxicol.* 21, 1698–1705.
- (6) Sakamoto, Y., Nakae, D., Fukumori, N., Tayama, K., Maekawa, A., Imai, K., Hirose, A., Nishimura, T., Ohashi, N., and Ogata, A. (2009) Induction of mesothelioma by a single intrascrotal administration of multi-wall carbon nanotube in intact male Fischer 344 rats. *J. Toxicol. Sci.* 34, 65–76.
- (7) Zhu, L., Chang, D. W., Dai, L., and Hong, Y. (2007) DNA damage induced by multiwalled carbon nanotubes in mouse embryonic stem cells. *Nano Lett.* 7, 3592–3597.
- (8) Donaldson, K., and Stone, V. (2003) Current hypotheses on the mechanisms of toxicity of ultrafine particles. *Ann. Ist. Super. Sanita* 39, 405–410.
- (9) Fenoglio, I., Greco, G., Tornatis, M., Muller, J., Raymundo-Pinero, E., Beguin, F., Fonseca, A., Nagy, J. B., Lison, D., and Fubini, B. (2008) Structural defects play a major role in the acute lung toxicity of multiwall carbon nanotubes: Physicochemical aspects. *Chem. Res. Toxicol.* 21, 1690–1697.
- (10) Jacobsen, N. R., Pojana, G., White, P., Moller, P., Cohn, C. A., Korsholm, K. S., Vogel, U., Marcomini, A., Loft, S., and Wallin, H. (2008) Genotoxicity, cytotoxicity, and reactive oxygen species induced by single-walled carbon nanotubes and C-60 fullerenes in the FE1-Muta (TM) mouse lung epithelial cells. *Environ. Mol. Mutagen.* 49, 476–487.
- (11) Zeni, O., Palumbo, R., Bernini, R., Zeni, L., Sarti, M., and Scarfi, M. R. (2008) Cytotoxicity investigation on cultured human blood cells treated with single-wall carbon nanotubes. *Sensors* 8, 488–499.
- (12) Kisin, E. R., Murray, A. R., Keane, M. J., Shi, X.-C., Schwegler-Berry, D., Gorelik, O., Arepalli, S., Castranova, V., Wallace, W. E., Kagan, V. E., and Shvedova, A. A. (2007) Single-walled carbon nanotubes: Geno- and cytotoxic effects in lung fibroblast V79 cells. *J. Toxicol. Environ. Health.* 70, 2071–2079.
- (13) Pacurari, M., Yin, X. J., Zhao, J., Ding, M., Leonard, S. S., Schwegler-Berry, D., Ducatman, B. S., Sbarra, D., Hoover, M. D., Castranova, V., and Vallathan, V. (2008) Raw single-wall carbon nanotubes induce oxidative stress and activate MAPKs, AP-1, NF-kappa B, and Akt in normal and malignant human mesothelial cells. *Environ. Health Perspect.* 116, 1211–1217.
- (14) Cradwick, P. D. G., Farmer, V. C., Russell, J. D., Masson, C. R., Wada, K., and Yoshinaga, N. (1972) Imogolite, a hydrated aluminium silicate of tubular structure. *Nature Phys. Sci.* 240, 187–189.
- (15) Farmer, V. C., Adams, M. J., Fraser, A. R., and Palmieri, F. (1983) Synthetic imogolite-properties synthesis, and possible applications. *Clay Minerals* 18, 459–472.

- (16) Farmer, V. C., Fraser, A. R., and Tait, J. M. (1977) Synthesis of imogolite-tubular aluminum silicate polymer. *J. Chem. Soc., Chem. Commun.*, 462–463.
- (17) Imamura, S., Hayashi, Y., Kajiwara, K., Hoshino, and H., Kaito, C. (1993) Imogolite—a possible new type of shape-selective catalyst. *Ind. Eng. Chem. Res.* 32, 600–603.
- (18) Ohashi, F., Wada, S. I., Suzuki, M., Maeda, M., and Tomura, S. (2002) Synthetic allophane from high-concentration solutions: nano-engineering of the porous solid. *Clay Minerals.* 37, 451–456.
- (19) Levard, C., Rose, J., Masion, A., Doelsch, E., Borschneck, D., Olivi, L., Dominici, C., Grauby, O., Woicik, J. C., and Bottero, J.-Y. (2008) Synthesis of large quantities of single-walled aluminogermanate nanotube. *J. Am. Chem. Soc.* 130, 5862–+.
- (20) Levard, C., Rose, J., Thill, A., Masion, A., Doelsch, E., Maillet, P., Spalla, O., Olivi, L., Cognigni, A., Ziarelli, F., and Bottero, J. Y. (2010) Formation and growth mechanisms of imogolite-like aluminogermanate nanotubes. *Chem. Mater.* 22, 2466–2473.
- (21) Maillet, P., Levard, C., Larquet, E., Mariet, C., Spalla, O., Menguy, N., Masion, A., Doelsch, E., Rose, J., and Thill, A. (2010) Evidence of double-walled Al-Ge imogolite-like nanotubes. A Cryo-TEM and SAXS investigation. *J. Am. Chem. Soc.* 132, 1208–+.
- (22) Yucelen, G. I., Choudhury, R. P., Vyalikh, A., Scheler, U., Beckham, H. W., and Nair, S. (2011) Formation of single-walled aluminosilicate nanotubes from molecular precursors and curved nanoscale intermediates. *J. Am. Chem. Soc.* 133, 5397–5412.
- (23) Ishikawa, K., Abe, S., Yawaka, Y., Suzuki, M., and Watari, F. (2010) Osteoblastic cellular responses to aluminosilicate nanotubes, imogolite using Saos-2 and MC3T3-E1 cells. *J. Ceram. Soc. Jpn.* 118, 516–520.
- (24) Nahm, W. K., Zhou, L., and Falanga, V. (2002) Sustained ability for fibroblast outgrowth from stored neonatal foreskin: a model for studying mechanisms of fibroblast outgrowth. *J. Dermatol. Sci.* 28, 152–158.
- (25) Proux, O., Biquard, X., Lahera, E., Menthonnex, J. J., Prat, A., Ulrich, O., Soldo, Y., Trevisson, P., Kapoujyan, G., Perroux, G., Taunier, P., Grand, D., Jeantet, P., Deleglise, M., Roux, J. P., and Hazemann, J. L. (2005) FAME: A new beamline for X-ray absorption investigations of very-diluted systems of environmental, material and biological interests. *Phys. Scr. T115*, 970–973.
- (26) Proux, O., Nassif, V., Prat, A., Ulrich, O., Lahera, E., Biquard, X., Menthonnex, J. J., and Hazemann, J. L. (2006) Feedback system of a liquid-nitrogen-cooled double-crystal monochromator: design and performances. *J. Synchrotron Radiat.* 13, 59–68.
- (27) Ravel, B., and Newville, M. (2005) ATHENA, ARTEMIS, HEPHAESTUS: data analysis for X-ray absorption spectroscopy using IFEFFIT. *J. Synchrotron Radiat.* 12, 537–541.
- (28) Tice, R. R., Agurell, E., Anderson, D., Burlinson, B., Hartmann, A., Kobayashi, H., Miyamae, Y., Rojas, E., Ryu, J. C., and Sasaki, Y. F. (2000) Single cell gel/comet assay: Guidelines for in vitro and in vivo genetic toxicology testing. *Environ. Mol. Mutagen.* 35, 206–221.
- (29) Bauer, E., Recknagel, R. D., Fiedler, U., Wollweber, L., Bock, C., and Greulich, K. O. (1998) The distribution of the tail moments in single cell gel electrophoresis (comet assay) obeys a chi-square (χ^2) not a gaussian distribution. *Mutat. Res., Fundam. Mol. Mech. Mutagen.* 398, 101–110.
- (30) Kirsch-Volders, M., Sofuni, T., Aardema, M., Albertini, S., Eastmond, D., Fenech, M., Ishidate, M., Kirchner, S., Lorge, E., Morita, T., Norppa, H., Surrallés, J., Vanhaever, A., and Wakata, A. (2004) Report from the in vitro micronucleus assay working group (vol 540, pg 153, 2003). *Mutat. Res., Genet. Toxicol. Environ. Mutagen.* 564, 97–100.
- (31) Kirsch-Volders, M., Elhajouji, A., Cundari, E., and VanHummelen, P. (1997) The in vitro micronucleus test: A multi-endpoint assay to detect simultaneously mitotic delay, apoptosis, chromosome breakage, chromosome loss and non-disjunction. *Mutat. Res., Genet. Toxicol. Environ. Mutagen.* 392, 19–30.
- (32) Creton, B., Bougeard, D., Smirnov, K. S., Guilment, J., and Poncelet, O. (2008) Molecular dynamics study of hydrated imogolite-2. Structure and dynamics of confined water. *PCCP.* 10, 4879–4888.
- (33) Lynch, I., and Dawson, K. A. (2008) Protein-nanoparticle interactions. *Nano Today* 3, 40–47.
- (34) Monopoli, M. P., Walczyk, D., Campbell, A., Elia, G., Lynch, I., Bombelli, F. B., and Dawson, K. A. (2011) Physical-chemical aspects of protein corona: relevance to in vitro and in vivo biological impacts of nanoparticles. *J. Am. Chem. Soc.* 133, 2525–2534.
- (35) Rausch, K., Reuter, A., Fischer, K., and Schmidt, M. (2010) Evaluation of nanoparticle aggregation in human blood serum. *Biomacromolecules* 11, 2836–2839.
- (36) Gratton, S. E. A., Ropp, P. A., Pohlhaus, P. D., Luft, J. C., Madden, V. J., Napier, M. E., and DeSimone, J. M. (2008) The effect of particle design on cellular internalization pathways. *Proc. Natl. Acad. Sci. U.S.A.* 105, 11613–11618.
- (37) Chithrani, B. D., and Chan, W. C. W. (2007) Elucidating the mechanism of cellular uptake and removal of protein-coated gold nanoparticles of different sizes and shapes. *Nano Lett.* 7, 1542–1550.
- (38) Kim, J. S., Song, K. S., Joo, H. J., Lee, J. H., and Yu, I. J. (2010) Determination of cytotoxicity attributed to multiwall carbon nanotubes (MWCNT) in normal human embryonic lung cell (WI-38) line. *J. Toxicol. Environ. Health.* 73, 1521–1529.
- (39) Stella, G. M. (2011) Carbon nanotubes and pleural damage: Perspectives of nanosafety in the light of asbestos experience. *Biointerphases* 6, P1–P17.
- (40) Zhang, Y., Wang, B., Meng, X., Sun, G., and Gao, C. (2011) Influences of acid-treated multiwalled carbon nanotubes on fibroblasts: proliferation, adhesion, migration, and wound healing. *Ann. Biomed. Eng.* 39, 414–426.
- (41) Mu, Q., Li, Z., Li, X., Mishra, S. R., Zhang, B., Si, Z., Yang, L., Jiang, W., and Yan, B. (2009) Characterization of protein clusters of diverse magnetic nanoparticles and their dynamic interactions with human cells. *J. Phys. Chem.* 113, 5390–5395.
- (42) Ehrenberg, M. S., Friedman, A. E., Finkelstein, J. N., Oberdoerster, G., and McGrath, J. L. (2009) The influence of protein adsorption on nanoparticle association with cultured endothelial cells. *Biomaterials.* 30, 603–610.
- (43) Lindberg, H. K., Falck, G. C. M., Suhonen, S., Vippola, M., Vanhala, E., Catalan, J., Savolainen, K., and Norppa, H. (2009) Genotoxicity of nanomaterials: DNA damage and micronuclei induced by carbon nanotubes and graphite nanofibres in human bronchial epithelial cells in vitro. *Toxicol. Lett.* 186, 166–173.
- (44) Jiang, J., Oberdoerster, G., and Biswas, P. (2009) Characterization of size, surface charge, and agglomeration state of nanoparticle dispersions for toxicological studies. *J. Nanopart. Res.* 11, 77–89.
- (45) Hussain, S. M., Hess, K. L., Gearhart, J. M., Geiss, K. T., and Schlagler, J. J. (2005) In vitro toxicity of nanoparticles in BRL 3A rat liver cells. *Toxicol. in Vitro* 19, 975–983.
- (46) Leroueil, P. R., Berry, S. A., Duthie, K., Han, G., Rotello, V. M., McNerny, D. Q., Baker, J. R., Jr., Orr, B. G., and Holl, M. M. B. (2008) Wide varieties of cationic nanoparticles induce defects in supported lipid bilayers. *Nano Lett.* 8, 420–424.
- (47) Kathiravan, A., Paramaguru, G., and Renganathan, R. (2009) Study on the binding of colloidal zinc oxide nanoparticles with bovine serum albumin. *J. Mol. Struct.* 934, 129–137.
- (48) Chen, M., and von Mikecz, A. (2005) Formation of nucleoplasmic protein aggregates impairs nuclear function in response to SiO₂ nanoparticles. *Exp. Cell Res.* 305, 51–62.
- (49) Kovacic, P., and Somanathan, R. (2010) Biomechanisms of nanoparticles (toxicants, antioxidants and therapeutics): electron transfer and reactive oxygen species. *J. Nanosci. Nanotechnol.* 10, 7919–7930.
- (50) Oberdoerster, G., Maynard, A., Donaldson, K., Castranova, V., Fitzpatrick, J., Ausman, K., Carter, J., Karn, B., Kreyling, W., Lai, D., Olin, S., Monteiro-Riviere, N., Warheit, D., and Yang, H. (2005) Screening Working, G.: Principles for characterizing the potential human health effects from exposure to nanomaterials: elements of a screening strategy. *Part. Fibre Toxicol.* 2, 8.
- (51) Petersen, E. J., and Nelson, B. C. (2010) Mechanisms and measurements of nanomaterial-induced oxidative damage to DNA. *Anal. Bioanal. Chem.* 398, 613–650.

- (52) Nel, A., Xia, T., Madler, and L., Li, N. (2006) Toxic potential of materials at the nanolevel. *Scienc.* 311, 622–627.
- (53) Shukla, R. K., Sharma, V., Pandey, A. K., Singh, S., Sultana, S., and Dhawan, A. (2011) ROS-mediated genotoxicity induced by titanium dioxide nanoparticles in human epidermal cells. *Toxicol. in Vitro* 25, 231–241.
- (54) Chaudiere, J., and Ferrari-Iliou, R. (1999) Intracellular antioxidants: from chemical to biochemical mechanisms. *Food Chem. Toxicol.* 37, 949–962.
- (55) Decome, L., De Meo, M., Geffard, A., Doucet, O., Dumenil, G., and Botta, A. (2005) Evaluation of photolyase (Photosome (R)) repair activity in human keratinocytes after a single dose of ultraviolet B irradiation using the comet assay. *J. Photochem. Photobiol., B* 79, 101–108.
- (56) Okamoto, Y., Hayashi, T., Matsunami, S., Ueda, K., Toda, C., Kawanishi, S., and Kojima, N. (2006) Formation of DNA damaging product from light-irradiated nonylphenol. *J. Health Sci.* 52, 91–95.